

Dalton Transactions

Accepted Manuscript



This is an *Accepted Manuscript*, which has been through the Royal Society of Chemistry peer review process and has been accepted for publication.

Accepted Manuscripts are published online shortly after acceptance, before technical editing, formatting and proof reading. Using this free service, authors can make their results available to the community, in citable form, before we publish the edited article. We will replace this *Accepted Manuscript* with the edited and formatted *Advance Article* as soon as it is available.

You can find more information about *Accepted Manuscripts* in the [Information for Authors](#).

Please note that technical editing may introduce minor changes to the text and/or graphics, which may alter content. The journal's standard [Terms & Conditions](#) and the [Ethical guidelines](#) still apply. In no event shall the Royal Society of Chemistry be held responsible for any errors or omissions in this *Accepted Manuscript* or any consequences arising from the use of any information it contains.

Notable Differences between Oxidized Diruthenium Complexes Bridged by Four Isomeric Diethynyl Benzodithiophene Ligands

Ya-Ping Ou^{†,‡,⊥}, Jing Zhang^{†,⊥}, Fuxing Zhang^{‡,§}, Daizhi Kuang^{‡,§}, František Hartl^{*,#}, Li Rao[†], Sheng Hua Liu^{*,†}

[†]Key Laboratory of Pesticide and Chemical Biology, Ministry of Education, College of Chemistry, Central China Normal University, Wuhan 430079, P.R. China

[‡]College of Chemistry and Material Science, Hengyang Normal University, Hengyang, Hunan 421008, P.R. China

[§]Key Laboratory of Functional Organometallic Materials of Hunan Province College, Hengyang Normal University, Hengyang, Hunan 421008, P.R. China

[#]Department of Chemistry, University of Reading, Whiteknights, Reading RG6 6AD, U.K.

*Corresponding authors:

E-mail: f.hartl@readig.ac.uk; chshliu@mail.ccnu.edu.cn

[⊥]These authors contributed equally to this work.

Abstract

Four new diruthenium complexes $[\{(\eta^5\text{-C}_5\text{Me}_5)\text{Ru}(\text{dppe})\}_2(\mu\text{-C}\equiv\text{C-L-C}\equiv\text{C})]$ featuring different bridging isomeric diethynyl benzodithiophenes viz. L = benzo[1,2-b;4,5-b']dithiophene (complex **1**), benzo[2,1-b;4,5-b']dithiophene (complex **2**), benzo[1,2-b;3,4-b']dithiophene (complex **3**) and benzo[1,2-b;4,3-b']dithiophene (complex **4**), were synthesized and characterized by molecular spectroscopic and crystallographic methods. The subtle changes in the molecular structure introduced by the diethynyl benzodithiophene isomers have a notable impact on the stability of the oxidized complexes and their absorption characteristics in the visible-NIR and IR spectral domains. Electronic properties of stable oxidized complexes $[\mathbf{1}]^{n+}$ and $[\mathbf{4}]^{n+}$ ($n = 1, 2$) were investigated by cyclic voltammetry, UV-vis-NIR and IR spectroelectrochemistry as well as DFT and TDDFT calculations. The results document the largely bridge-localized character of the oxidation of parent **1** and **4**.

Cations $[2]^+$ and $[3]^+$ are too unstable at ambient temperature to afford their unambiguous characterization. UV-vis-NIR absorption spectral data combined with TDDFT calculations (BLYP35) reveal that the broad electronic absorption of $[1]^+$ and $[4]^+$ in the NIR region has a mixed intraligand π - π^* and MLCT character, with similar contribution from their spin-delocalized *trans* and *cis* conformers. A spin-localized (mixed-valence) rotamer was only observed for $[1]^+$ at ambient temperature as a minor component on the time scale of IR spectroscopy.

Keywords: Diruthenium Complex; Spectroelectrochemistry; Benzodithiophene Isomer; Molecular Bridge; Ethynyl Linker; DFT Calculations

Introduction

Homobimetallic complexes $[\{ML_n\}_2(\mu-BL)]^{n+}$ (BL = bridging ligand) with two redox-active termini, bridged by π -conjugated organic ligands, have received increasing interest for their interesting electronic, magnetic and optical properties^[1] exploited to design and fabricate electronic devices on the molecular level^[2]. The principal objective follows the concept of so-called ‘organometallic molecular wires’ capable of directional intramolecular electron transfer. As the physical properties of ‘organometallic molecular wires’ are determined mainly by the structure of the bridging ligand, suitable rigid-rod molecular bridges can provide controllable electronic coupling and a charge transfer pathway^[2c, 3]. Introducing redox-active metal termini at the rigid-rod bridging ligands can provide defined donor-bridge-acceptor (D-B-A) sites and promote the electron hopping in the mixed-valence state^[2a, 4]. In the last decade, plentiful ethynyl-terminated ligands featuring a conjugated aromatic core were introduced as bridges in diverse homobimetallic complexes and the corresponding redox characteristics of these system have been reported^[5-8]. Dinuclear complexes with the $Cp^*Fe(dppe)$ ($Cp^* = \eta^5-C_5Me_5$; $dppe = 1,2$ -diphenylphosphinoethane) or ferrocenyl (Fc) redox-active centers typically exhibit largely metal-ethynyl-localized oxidation creating IVCT electronic absorption in the NIR spectral region^[5-6]. On the other hand, dinuclear complexes with

Cp*Ru(dppe) or RuCl(dppe)₂ termini feature a strongly redox non-innocent bridge^[7-8]. The different anodic behavior of the two types of complexes may be attributed to the varying extent of the interaction between the d_π-type orbitals at the metal termini and the frontier π-orbitals of the bridging ligands. In general, the frontier orbitals of the ruthenium ethynyl complexes exhibit a limited metallic character^[2e, 2f, 7-9]. The molecular bonding properties of the bridging ligands (donor capacity, the extent of conjugation, transversal and longitudinal parameters) control their participation in the oxidation process^[7]. Recently, several experimental and computational studies have also suggested that the orientation of the bridging conjugated core relative to the metal-ethynyl centers and the mutual conformation of the ligated metal termini play an important role in controlling the metal vs bridging ligand characters of the redox processes in the $[\{ML_n\}_2(\mu-BL)]$ systems (the Parthey-Low concept). The characteristic broad NIR absorptions and complex $\nu(C\equiv C)$ stretching patterns of the corresponding radical cations are then modelled by the dynamic behavior of the molecular bridge^[10-14, 26c].

Fused heteroaromatic compounds based on thiophene represent an interesting class of electronic materials utilized for organic semiconductors and field-effect transistors due to their high operational stabilities at ambient conditions, high charge-carrier mobilities and economically feasible syntheses^[15-18]. In 2010, isomeric benzodithiophene building blocks were used by Müllen et al.^[19] to construct different backbone curvature polymers and investigate their device properties. Experimental results have indicated that charge-carrier mobilities in these polymers depend largely on the configuration of the benzodithiophene building blocks. Subsequently, in 2014 Ogawa et al. synthesized diferrocenyl complexes bridged by *anti*- and *syn*-benzodithiophenes and investigated their electrochemical oxidation. They observed two poorly resolved anodic waves reflecting the negligible inter-ferrocenyl electronic communication because of the long Fe–BL–Fe distances^[20].

To date, however, there have been no other reports on dinuclear complexes with metal centers tightly linked to isomeric benzodithiophene ligands to test their

conjugated bonding properties and tune the anodic behavior. With this goal in mind, we have bound the reference redox-active $\text{Cp}^*\text{Ru}(\text{dppe})\text{C}\equiv\text{C}-$ terminal units to benzo[1,2-b;4,5-b']dithiophene (complex **1**), benzo[2,1-b;4,5-b']dithiophene (complex **2**), benzo[1,2-b;3,4-b']dithiophene (complex **3**) and benzo[1,2-b;4,3-b']dithiophene (complex **4**), as shown in Chart 1. The molecular structures of the target complexes were fully characterized by NMR spectroscopy and X-ray diffraction (**1** - **3**). The conjugated bonding and redox properties were investigated by combined methods of cyclic voltammetry, IR and UV-Vis-NIR spectroelectrochemistry and density functional theory calculations.

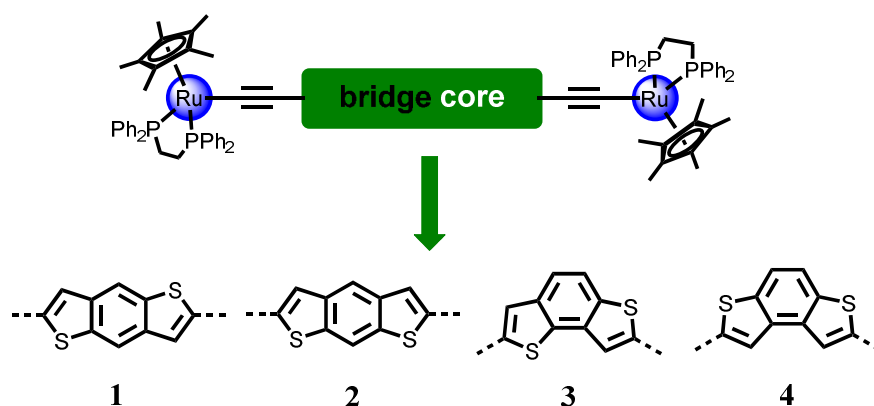


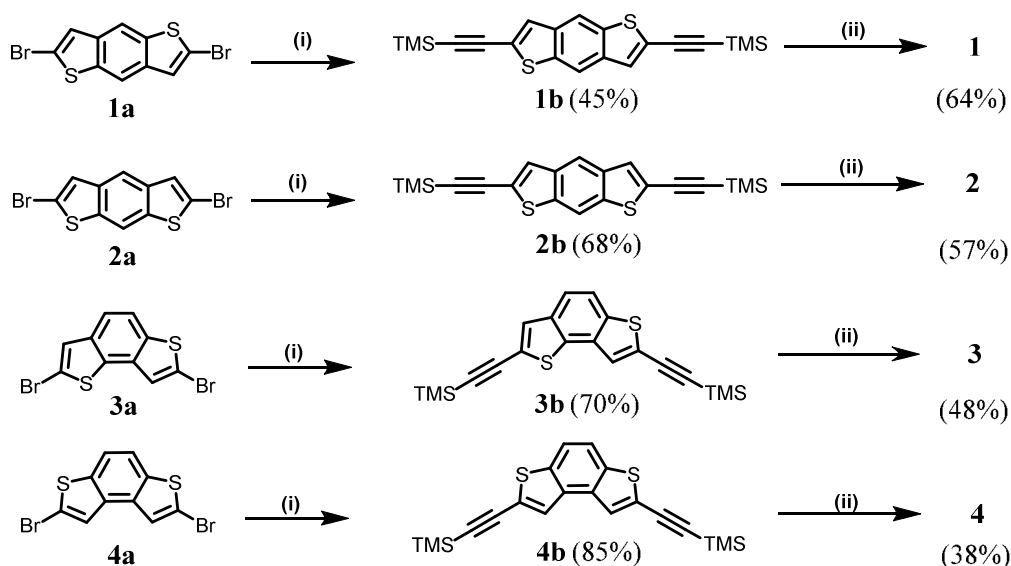
Chart 1. Isomeric diethynyl benzodithiophene-bridged diruthenium complexes **1** - **4** studied in this work.

Results and Discussion

Syntheses and Characterization

The general synthetic route to isomeric diethynyl benzodithiophene-bridged diruthenium complexes **1** - **4** is outlined in Scheme 1. Intermediates **1b** - **4b** were obtained in yields ranging between 45-85%, using Pd/Cu-catalyzed Sonogashira coupling reactions between bromo-substituted precursors **1a** - **4a** (see Experimental) and trimethylsilyl acetylene, respectively. The target molecules **1** - **4** with half-sandwich termini $\text{Cp}^*\text{Ru}(\text{dppe})$ were conveniently prepared by fluoride-induced desilylmethallation of trimethylsilyl-protected acetylenes **1b** - **4b**^[7b]. Pure **1** - **4** were obtained by filtration and recrystallization from $\text{CH}_2\text{Cl}_2/n$ -hexane and characterized

by conventional spectroscopic methods and single-crystal X-ray diffraction. IR spectra of **1** - **4** exhibit a single $\nu(\text{C}\equiv\text{C})$ absorption band near 2050 cm^{-1} . In the ^1H NMR spectra, the methyl groups of Cp^* resonate as singlets near 1.60 ppm and the methylene groups of the dppe ligands as two broad signals near 2.10 ppm and 2.70 ppm. In the ^{13}C NMR spectra of **1** - **4**, multiplets or broad $\text{Ru}-\text{C}\equiv$ resonance signals (under the influence of the nearby phosphorus nuclei) were observed. The corresponding ^{31}P NMR spectra show dppe resonances between 79-80 ppm.



Scheme 1. Synthetic paths to diethynyl benzodithiophene-bridged diruthenium complexes **1** - **4**. Reagents and conditions: (i) TMSA, $[\text{Pd}(\text{PPh}_3)_4]$, CuI, THF/ Et_3N or $(i\text{Pr})_2\text{NH}$; (ii) $[\text{Cp}^*\text{RuCl}(\text{dppe})]$, KF, $\text{CH}_3\text{OH}/\text{THF}$, reflux for 24h.

Crystal Structures of Complexes **1**, **2** and **3**

Molecular structures of **1** - **3** (obtained as solvates in the case of **1** and **3**, see Experimental) have been determined by single-crystal X-ray diffraction analyses^[21] (Figures 1-3). Details of the data collection and refinement are presented in Table S1 (Supporting Information). Selected bond lengths and angles from crystal structures of **1** - **3** and DFT-optimized truncated model structures $[\mathbf{1-H}]^{n+}$ - $[\mathbf{4-H}]^{n+}$ ($n = 0, 1, 2$) are provided in Table 1 and Tables S2-S4 (Supporting Information). The extension “-H” indicates that the $\eta^5\text{-C}_5\text{Me}_5$ (Cp^*) and dppe ligands in **1-4** were replaced by

η^5 -C₅H₅ (Cp) and two PH₃ ligands, respectively (vide infra). The three crystallized diruthenium complexes consist of the Cp*Ru(dppe) termini linked to the diethynyl benzodithiophene chain by a Ru–C σ -bond. Similar to previously reported complexes^[7a, 7b, 22a], these molecules exhibit a pseudooctahedral geometry. The C≡C bond lengths in **1–3** are near 1.20 Å. The Ru–C≡ distance in complexes **1–3** are 2.015 Å, 1.985 Å and 2.002 Å, respectively. A comparison of the Ru–P bond lengths reveals an average value of 2.27 Å. Simulated oxidation of model complexes [**1-H**] and [**4-H**] to [**1-H**]²⁺ and [**4-H**]²⁺ all caused elongation of the C≡C and Ru–P bonds, together with shortening of the Ru–ethynyl and ethynyl–thiophene bonds, which is ascribed to a contribution from the cumulenic, {Ru=C=C=C}⁺ valence form^[7, 27a].

The two Ru atoms and benzo[1,2-b;4,5-b']dithiophene in **1** are not completely coplanar, the bond angle Ru(1)–C(37)–C(38) being 177.36°. On the other hand, complex **2** exhibits a very rigid structure where the two Ru atoms, C(37)–C(38) and benzo[2,1-b;4,5-b']dithiophene are almost coplanar, the bond angle Ru(1)–C(37)–C(38) reaching 179.29°. The distances between the two ruthenium atoms in **1** and **2** are nevertheless close to 16.21 Å in both cases. In **3**, the two Cp*Ru(dppe) terminal groups exhibit a weak distortion resulting from the shortening of the space distance between the ruthenium atoms (13.72 Å).

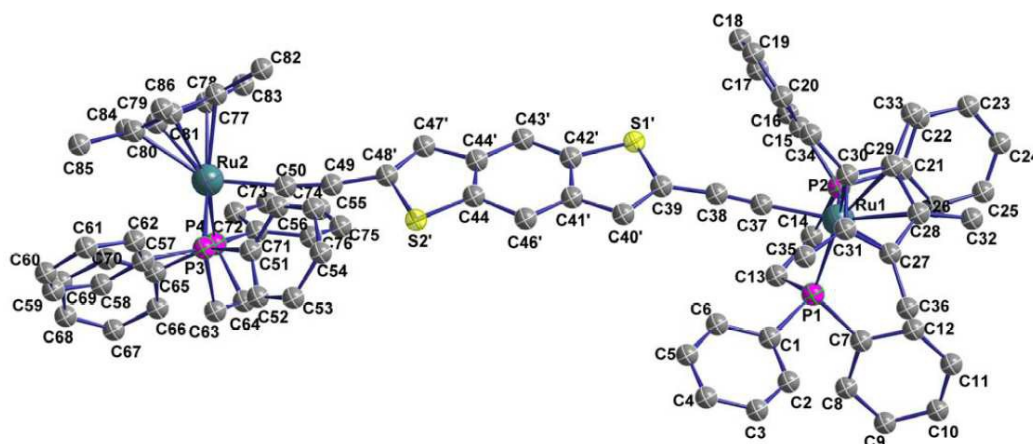


Figure 1. Molecular structure of complex **1** showing the atom labelling scheme. Hydrogen atoms are omitted for clarity.

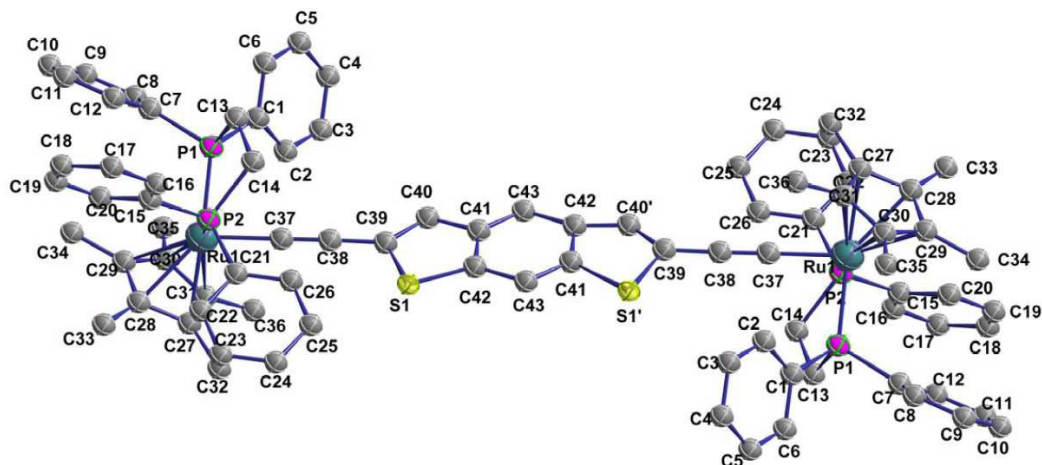


Figure 2. Molecular structure of complex **2** showing the atom labelling scheme. Hydrogen atoms are omitted for clarity.

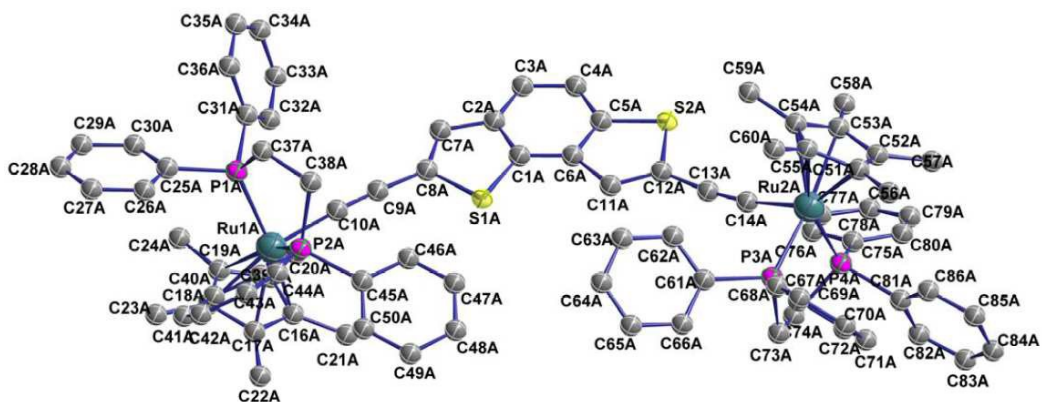


Figure 3. Molecular structure of complex **3** showing the atom labelling scheme. Hydrogen atoms are omitted for clarity.

Table 1. Selected Bond Lengths (Å) and Angles (deg) in the Crystal Structure of **1** and the DFT-Optimized Model Structures $[\mathbf{1-H}]^{n+}$ ($n = 0, 1, 2$)

Parameter	1	$[\mathbf{1-H}]$	$[\mathbf{1-H}]^+$	$[\mathbf{1-H}]^{2+}$
Ru(1)-C(37)	2.015	2.009	1.966	1.925
Ru(1)-P(1, 2)	2.263, 2.276	2.279, 2.281	2.300, 2.301	2.321, 2.323
C(37)-C(38)	1.181	1.229	1.241	1.254
C(38)-C(39)	1.436	1.402	1.377	1.356
C(39)-C(40)	1.322	1.372	1.399	1.428
C(40)-C(41)	1.423	1.437	1.409	1.384
C(41)-C(46)	1.390	1.404	1.418	1.433
C(41)-C(42)	1.390	1.433	1.446	1.460
C(42)-S(1)	1.725	1.756	1.757	1.759

S(1)-C(39)	1.744	1.787	1.780	1.776
P(1)-Ru(1)-P(2)	83.56	93.10	92.47	91.20
Ru(1)-C(37)-C(38)	177.36	178.06	177.51	177.20
C(37)-C(38)-C(39)	174.06	177.16	176.93	176.29

Electrochemical Studies

The redox properties of complexes **1** - **4** were first probed by cyclic voltammetry (CV) and square wave voltammetry (SWV) (Figure 4). The anodic scans have revealed that **1** - **4** undergo two consecutive one-electron oxidation processes. The CV plots show that both anodic steps of **1** and **4** are chemically and electrochemically reversible, pointing to stability of the corresponding mono- and dications. In sharp contrast, the first anodic wave of **2** is totally irreversible. Complex **3** represents an intermediate case, cation $[3]^+$ being largely detectable at ambient temperature during the reverse cathodic scan on the time scale of seconds. Detailed electrochemical data are given in Table 2. The oxidation potential of **4** is significantly more positive compared to those of **1** - **3**; notably, this trend was not reproduced by DFT calculations of the corresponding HOMO energies (see Supporting Information). In linear benzodithiophene-bridged bimetallic complexes **1** and **2**, the potential difference between the two anodic waves ($\Delta E_{1/2}$) varies from 140 mV for **1** to 108 mV for **2**; however, the smaller anodic peak-to-peak separation in the latter case may be caused (at least in part) by the irreversible nature of the oxidation. The non-linear benzodithiophene-bridged bimetallic complexes, **3** and **4**, exhibit again similar $\Delta E_{1/2}$ values as complex **1**. Therefore, we conclude that the redox properties in the studied series of diethynyl benzodithiophene complexes and the stability of their radical cations depend notably on the configuration of the bridging ligand core.^[8a, 22-25] Singly oxidized $[2]^+$ and $[3]^+$ are unstable in the electrolyte solution according to the CV results, as also confirmed by the corresponding spectroelectrochemical experiments described in the following section.

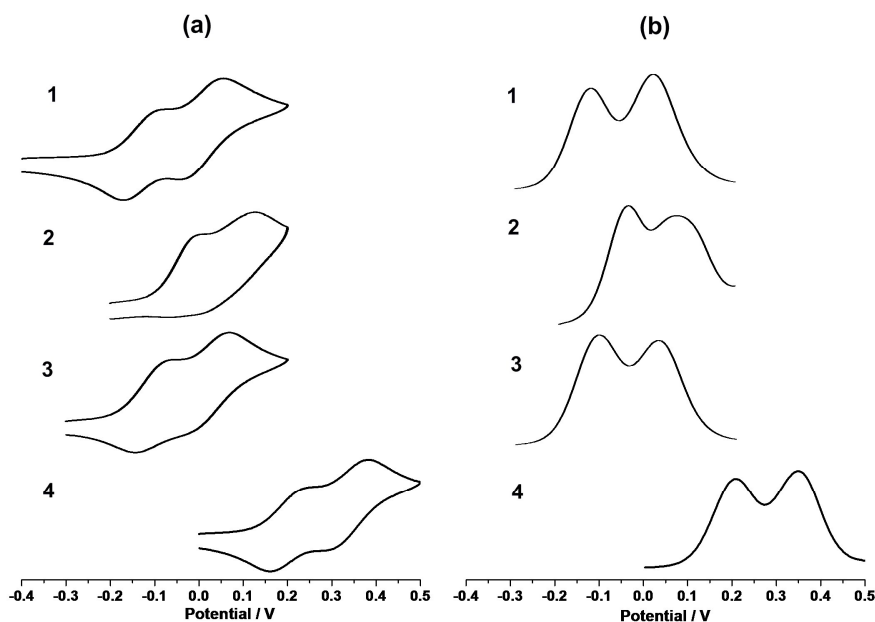


Figure 4. (a) Cyclic voltammograms (CV) of complexes **1-4** in $\text{CH}_2\text{Cl}_2/\text{Bu}_4\text{NPF}_6$ at $\nu = 10^{-1} \text{ V s}^{-1}$ and (b) anodic square-wave voltammograms (SWV) of **1 - 4** at $f = 10 \text{ Hz}$ ($t_p = 25 \text{ mV}$). The potential values are scaled against the $E_{1/2}$ value of the standard ferrocene/ferrocenium redox couple.

Table 2. Electrochemical Data for Complexes **1 - 4**^a

Complex	$E_{1/2}^{(1)}$ (V) (ΔE_p)	$E_{1/2}^{(2)}$ (V) (ΔE_p)	$\Delta E_{1/2}$ (mV) ^b
1	-0.124 (0.08)	0.016 (0.09)	140
2	-0.040 ^c	--	--
3	-0.108 (0.07)	0.025 (0.08)	133
4	0.196 (0.08)	0.336 (0.08)	140

^a Anodic potentials vs Fc/Fc^+ obtained from cyclic voltammograms recorded at 293 K in dichloromethane/ 10^{-1} M Bu_4NPF_6 . Additional electrochemical processes observed at higher electrode potentials were not examined further. ^b $\Delta E_{1/2} = E_{1/2}^{(2)} - E_{1/2}^{(1)}$ denotes the potential difference between the two reversible anodic processes. ^c $E_{p,a}$ - totally irreversible oxidation of **2**; the unassigned secondary product oxidizes at $E_{p,a} = 0.068 \text{ V}$ ($\nu = 100 \text{ mV s}^{-1}$).

IR Spectroelectrochemical Studies

IR spectroelectrochemistry was employed to investigate, on the short IR vibrational time scale (10^{-12} s $^{-1}$)^[7a, 26], the degree of involvement of the metal center and the bridging ligand in the anodic processes shown by **1** - **4** in the preceding section, and to probe the long-term stability of the different oxidation states. The IR spectroelectrochemical measurements in the dichloromethane/ Bu_4NPF_6 electrolyte were performed within optically transparent thin-layer electrochemistry (OTTLE) cells (see Experimental). Hereinafter, we mainly focus on the results recorded for reversibly oxidized complexes **1** and **4**. In order to confirm the difference in the stability revealed by CV (see above), the one-electron oxidation of **1**, **2** and **4** was also carried out at 223 K. Complexes $[\mathbf{1}]^{2+}$ were $[\mathbf{4}]^{2+}$ were found insoluble at the low temperature.

The plots of IR spectra obtained in the IR $\nu(\text{C}\equiv\text{C})$ and NIR regions for complexes $[\mathbf{1}]^{n+}$ and $[\mathbf{4}]^{n+}$ ($n = 0, 1, 2$) at 298 K and for complex $[\mathbf{1}]^{n+}$ ($n = 0, 1$) at 223 K are depicted in Figures 5 and 6 and Figure S1, respectively. Corresponding characteristic $\nu(\text{C}\equiv\text{C})$ wavenumbers are listed in Table 3. In detail, one-electron oxidation of **1** and **4** to corresponding stable cations replaced the single $\nu_{\text{as}}(\text{C}\equiv\text{C})$ band of the parent complexes at ca. 2045 cm^{-1} by two intense $\nu(\text{C}\equiv\text{C})$ bands at 1979 (s, br) and 1938 (vs) cm^{-1} ($\Delta\tilde{\nu} = 41\text{ cm}^{-1}$) for $[\mathbf{1}]^+$ (Figure 5) and at 2000 (vs, br) and 1914 (vs) cm^{-1} ($\Delta\tilde{\nu} = 86\text{ cm}^{-1}$) for $[\mathbf{4}]^+$ (Figure 6), along with the appearance of new broad $\pi\text{-}\pi^*/\text{MLCT}$ electronic absorption in the NIR region (below 6000 cm^{-1}), which will be analyzed in the following two sections. The intense $\nu(\text{C}\equiv\text{C})$ absorption of the cationic complexes corresponds to the symmetric and asymmetric stretching modes of the oxidized $-\text{C}\equiv\text{C}-\text{core}^+-\text{C}\equiv\text{C}-$ bridge, gaining intensity from the vibronic coupling to the low-lying MLCT electronic transitions.^[7a] The $\nu(\text{C}\equiv\text{C})$ shifts upon the one-electron oxidation and the $\Delta\tilde{\nu}$ values observed for $[\mathbf{1}]^+$ and $[\mathbf{4}]^+$ strongly resemble those for cationic congeners with 5,5'-linked 2,2'-bithiophene ($\Delta\tilde{\nu} = 49\text{ cm}^{-1}$) and 5,5''-linked 2,2':5',2''-terthiophene ($\Delta\tilde{\nu} = 87\text{ cm}^{-1}$), respectively, cores of the diethynyl-terminated bridging ligands.^[7b] An intermediate position with regard to the

$\nu(\text{C}\equiv\text{C})$ shifts and the $\Delta\tilde{\nu}$ value (63 cm^{-1}) is allocated to another derivative with a diethynyl carbazole bridge.^[7c] In all these published cases the entire diethynyl-aromatic bridge has been found to participate heavily in the one-electron oxidation of the neutral parent complex. Cations $[\mathbf{1}]^+$ and $[\mathbf{4}]^+$ with the isomeric diethynyl benzodithiophene bridges (Chart 1) differ in the characteristic low-energy $\pi\text{-}\pi^*/\text{MLCT}$ electronic absorptions tailing into the mid-IR region (Figures 5 and 6, left), which appear to have significant impact on the relative intensity and separation of the $\nu(\text{C}\equiv\text{C})$ bands. The lower the energy of the NIR electronic absorption the larger is the $\Delta\tilde{\nu}$ value and the higher is the relative intensity of the symmetric $\text{--C}\equiv\text{C--core}^+\text{--C}\equiv\text{C--}$ stretching mode. Notably, the same dependence is seen in the literature for a series of analogous monocationic diruthenium diethynyl complexes with an oligothiophene core (T_n)^[7b] instead of isomeric benzodithiophene: for T_1 , T_2 and T_3 , the $\Delta\tilde{\nu}$ value increases from $< 10\text{ cm}^{-1}$ to 49 cm^{-1} and 87 cm^{-1} , whereas the maximum of the lowest-lying absorption band shifts from 10750 cm^{-1} to 7050 cm^{-1} and 5950 cm^{-1} , respectively. Further research is needed for this family of diruthenium complexes with different redox-active diethynyl bridge cores to decide whether these trends represent a more general rule.

The clear appearance of the weak $\nu(\text{C}\equiv\text{C})$ band at 2042 cm^{-1} in the IR spectrum of $[\mathbf{1}]^+$ at 293 K (Figure 5) reflects thermal population of a less stable cationic rotamer featuring a distinct localized electronic character, as concluded with a reference to results of recent experimental and DFT studies published in this area by Low and Kaupp^[11-14], and verified by Lapinte^[5c, 10], Hartl and Liu^[26c] and Lang^[5d]. Lowering the temperature to 223 K resulted in disappearance of this valence-localized rotamer (Figure S1).

The IR $\nu(\text{C}\equiv\text{C})$ and NIR spectral changes recorded during the oxidation of neutral complex $\mathbf{2}$ in CH_2Cl_2 at 223 K are shown in Figure S2. The decrease of the parent $\nu(\text{C}\equiv\text{C})$ absorption at 2045 cm^{-1} is accompanied by appearance of two low-intensity bands at 1943 and 1877 cm^{-1} and NIR absorption between $7000\text{--}2000\text{ cm}^{-1}$. Whereas the NIR absorption resembles that of $[\mathbf{4}]^+$ (Figure 6), its intensity is too

low to be attributed to largely bridge-oxidized $[2]^+$, which also applies for the low $\nu(\text{C}\equiv\text{C})$ values (cm^{-1}). Chemical oxidation of **2** with ferrocenium hexafluorophosphate gave very similar results. These data afford convincing evidence against the formation of stable 2^+ in the electrolyte solution, in line with the irreversible nature of the anodic CV response (Figure 4).

Further oxidation of $[1]^+$ and $[4]^+$ at 293 K resulted in two weak $\nu(\text{C}\equiv\text{C})$ bands at 1972 and 1906 cm^{-1} for $[1]^{2+}$ and at 1974 and 1904 cm^{-1} for $[4]^{2+}$ (Figures 5 and 6, respectively). Again, this $\Delta\tilde{\nu}$ separation closely resembles the symmetric (1971(m-w) cm^{-1}) and asymmetric (1917(m) cm^{-1}) $\nu(\text{C}\equiv\text{C})$ signatures of the core-oxidized diethynyl bridge previously reported for the congeneric dication with the redox non-innocent diethynyl terthiophene (T_3) bridge.^[7b] At the same time, the NIR absorption of $[1]^+$ and $[4]^+$ below 6000 cm^{-1} was replaced upon the conversion to the corresponding dications with a new NIR absorption at ca. 11000 and 10000 cm^{-1} , respectively (Figures 5-7 and S4 and (left)). More details on the electronic absorption in the redox series are presented in the following UV-vis-NIR spectroelectrochemical section.

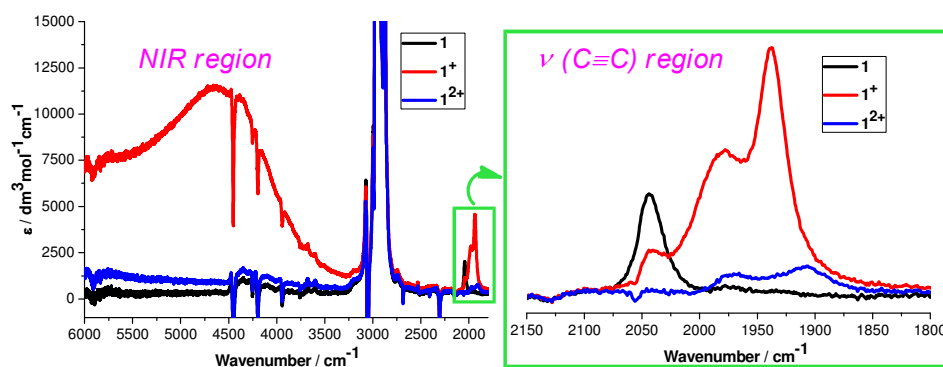


Figure 5. Spectral changes in the IR $\nu(\text{C}\equiv\text{C})$ (right) and NIR-IR (left) regions recorded for complexes $[1]^{n+}$ ($n = 0$ (black), 1 (red), 2 (blue)) electrochemically generated in $\text{CH}_2\text{Cl}_2/10^{-1}$ M Bu_4NPF_6 at 293 K within an OTTL cell.

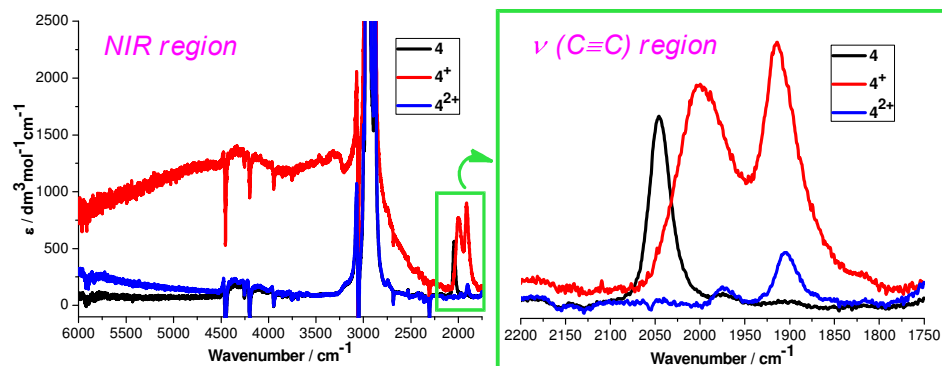


Figure 6. Spectral changes in the IR $\nu(\text{C}\equiv\text{C})$ (right) and NIR-IR (left) regions recorded for complexes $[\mathbf{4}]^{n+}$ ($n = 0$ (black), 1 (red), 2 (blue)) electrochemically generated in $\text{CH}_2\text{Cl}_2/10^{-1}$ M Bu_4NPF_6 at 293 K within an OTTLE cell.

Table 3. IR $\nu(\text{C}\equiv\text{C})$ Wavenumbers (cm^{-1}) of $[\mathbf{1}]^{n+}$ and $[\mathbf{4}]^{n+}$ ($n = 0, 1, 2$) in $\text{CH}_2\text{Cl}_2/10^{-1}$ M Bu_4NPF_6 .

Complex	$n = 0$	$n = 1$	$n = 2$
$[\mathbf{1}]^{n+}$	2044(s)	2042(w), 1979(s), 1938(vs)	1972(vw), 1906(w)
	2044(s) ^a	1985(s), 1940(vs) ^a	^b
$[\mathbf{4}]^{n+}$	2046(s)	2000(s), 1914(s)	1974(vw), 1904(w)
	2046(s) ^a	2006(s), 1917(s) ^a	^b

^a At $T = 223$ K. ^b No data available due to poor solubility of the dication at low temperature.

UV-vis-NIR Spectroelectrochemical Studies

In order to better understand the electronic and bonding properties of $[\mathbf{1}]^{n+}$ (Figure 7) and $[\mathbf{4}]^{n+}$ (Figure S4, Supporting Information), UV-vis-NIR absorption spectra of the complexes stable in the three oxidation states ($n = 0, 1, 2$) were collected at ambient temperature using the OTTLE cell. UV-vis absorption spectra of neutral complexes **2** and **3** in CH_2Cl_2 are shown in Figure S3 (Supporting Information). The wavenumbers of absorption maxima and molar absorptivities are listed in Table 4.

The electronic absorption spectra of neutral complexes **1** - **4** are dominated by intense $\pi\text{-}\pi^*$ absorptions between $28000\text{--}23000$ cm^{-1} (355–435 nm) which largely

originate from the diethynyl benzodithiophene parts, and some MLCT absorptions.^[11, 13, 23, 26c, 27, 28] The gradual one-electron oxidation to $[1]^+$ and $[4]^+$ results in decay of the intense absorption bands at 24000 cm^{-1} (415 nm) and 23000 cm^{-1} (435 nm), respectively, while new fairly weak absorption bands emerge in the visible region between $20000\text{--}10000\text{ cm}^{-1}$ (650–835 nm) and also in the NIR region between $10000\text{--}3300\text{ cm}^{-1}$ (1000–3000 nm). The fairly weak extended NIR-IR electronic absorption of $[4]^+$ can conveniently be presented by combining Figures 6 and S4. Absorption bands in the visible region are assigned to $L'(\text{Cp}^* \text{ and dppe})\rightarrow\text{MCT}$ and $\text{M}\rightarrow\text{L}(\text{bridge})\text{CT}$ electronic transitions. The broad absorption of $[1]^+$ and $[4]^+$ in the NIR region may be composed of several absorption bands belonging to conformers of $[1]^+$ and $[4]^+$ with different orientation of the bridging ligand (π -system) relative to the metal units^[10-14, 26c], having intraligand $\pi\text{-}\pi^*$ and MLCT characters. This assignment is in agreement with TDDFT results in the following section.

When $[1]^+$ and $[4]^+$ were further oxidized into corresponding stable dications $[1]^{2+}$ and $[4]^{2+}$, the low-lying NIR absorption disappeared (Figures 5 and 6) and a new absorption band appeared at 11090 cm^{-1} (900 nm) for $[1]^{2+}$ and 9830 cm^{-1} (1017 nm) for $[4]^{2+}$, tailing into the NIR region (Figure 7 and Figure S4). Such intense electronic transitions between 700–1200 nm are characteristic for closely related dications described in the literature^[7a-c, 8, 12, 26c]; they also may be attributed to MLCT/ $\pi\text{-}\pi^*$ transitions.

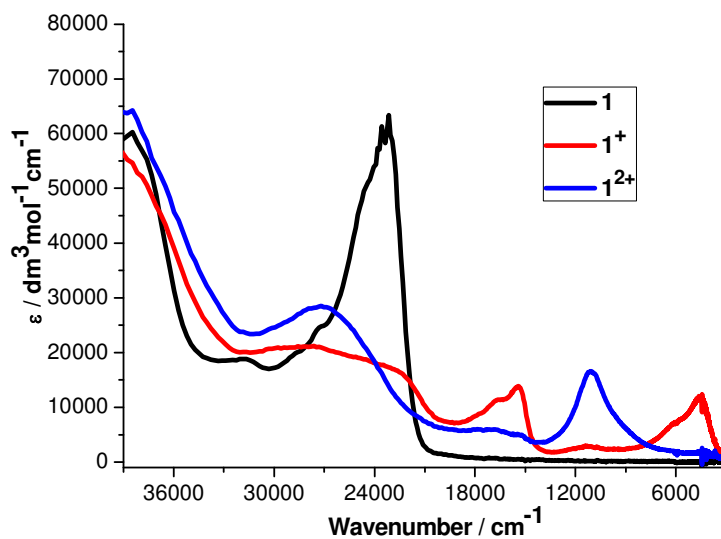


Figure 7. The UV-vis-NIR spectra of $[\mathbf{1}]^{n+}$ ($n = 0, 1, 2$) recorded by in situ oxidation of **1** in dichloromethane at 293 K with in an OTTLE cell.

Table 4. UV-vis-NIR Absorption Data for $[\mathbf{1}]^{n+}$, $[\mathbf{4}]^{n+}$ ($n = 0, 1, 2$) and Neutral Complexes **2** and **3**

Complex	$\tilde{\nu}_{\max}$ (cm^{-1}) (ϵ_{\max} ($\text{dm}^3 \text{mol}^{-1} \text{cm}^{-1}$)) ^a
1	23160 (61600)
$[\mathbf{1}]^+$	16700 (11700), 15380 (14100), 11140 (3200), 6000 (7400), 4540 (12400)
$[\mathbf{1}]^{2+}$	27020 (28700), 17000 (6500), 11090 (16800)
2	28060 (45350), 24630 (46700)
3	26700 (38900)
4	24040 (36300)
$[\mathbf{4}]^+$	27910 (24800), 17700 (6600), 12080 (4200), 4300 (2000), 3200 (2500)
$[\mathbf{4}]^{2+}$	28570 (20700), 20670 (13500), 13024 (6100), 9830 (10150)

^a Dichloromethane, 293 K.

DFT and TDDFT Calculations

To assist in the determination of the electronic structures, DFT calculations were performed on truncated models $[\mathbf{1-H}]^{n+}$, $[\mathbf{2-H}]^{n+}$, $[\mathbf{3-H}]^{n+}$ and $[\mathbf{4-H}]^{n+}$ ($n = 0, 1, 2$) at the B3LYP/3-21G* level of theory, the extension “-H” indicating that $\eta^5\text{-C}_5\text{Me}_5$ and dppe ligands in **1-4** were replaced by $\eta^5\text{-C}_5\text{H}_5$ and two PH_3 ligands, respectively. Next, representative non-truncated models of stable monocations $[\mathbf{1}]^+$ and $[\mathbf{4}]^+$ were selected for DFT calculations of possible different bridge conformations (rotamers) by using the BLYP35/6-31G* functional. These computational methods were commonly adopted for similar systems in the literature^[7-14, 21, 26]. Selected frontier orbitals with electron density distributions in models $[\mathbf{1-H}]^{n+}$ - $[\mathbf{4-H}]^{n+}$ ($n = 0, 1, 2$), based on the B3LYP/3-21G* method, are shown in Figure 8 and Figures S5-S7 (Supporting Information). Orbital energies and contributions based on the Mulliken population analysis of complexes $[\mathbf{1-H}]^{n+}$ - $[\mathbf{4-H}]^{n+}$ ($n = 0, 1, 2$) are delineated in Tables S5-S16 (Supporting Information).

The DFT calculations indicate that the lowest unoccupied molecular orbitals (LUMOs) of all neutral models $[\mathbf{1-H}]$ - $[\mathbf{4-H}]$ reside dominantly on one of the $\text{CpRu}(\text{PH}_3)_2$ fragments. The highest occupied molecular orbitals (HOMOs) are delocalized over the metal component and the diethynyl benzodithiophene backbone, all having dominant bridging ligand characters: $[\mathbf{1-H}]$ 80%; $[\mathbf{2-H}]$ 74%; $[\mathbf{3-H}]$ 84%; $[\mathbf{4-H}]$ 84%. The benzodithiophene core contributes with 50-60%, with the exception of complex $[\mathbf{2-H}]$ (44%) showing at the same time a pronounced asymmetric distribution of the HOMO over the Ru-ethynyl units (20% vs 30%). The HOMO of $[\mathbf{1-H}]$ has higher energy (-4.22 eV) than that of $[\mathbf{2-H}]$ (-4.46 eV), complying with the slightly less negative oxidation potential of **1** compared to **2**. However, the variation in the oxidation potentials for the whole series **1-4** (Table 2) has not been particularly well reproduced by the calculated HOMO energies; this applies especially for complex **4** oxidizing significantly more positively than predicted by the fairly high HOMO energy (-4.33 eV). Obviously, the studied series presents a challenge for the DFT treatment.

Considering the oxidized model complexes $[\mathbf{1-H}]^+$ - $[\mathbf{4-H}]^+$ and $[\mathbf{1-H}]^{2+}$ - $[\mathbf{4-H}]^{2+}$,

the β -LUSO of the monocations and the LUMO of the dications show higher metal contributions compared to the corresponding HOMO of the neutral precursors, which is most pronounced for non-linear $[3-H]^{n+}$ and $[4-H]^{n+}$ ($n = 0, 1, 2$). These frontier orbitals feature a symmetric distribution, which also applies to the oxidized forms of $[2-H]$.

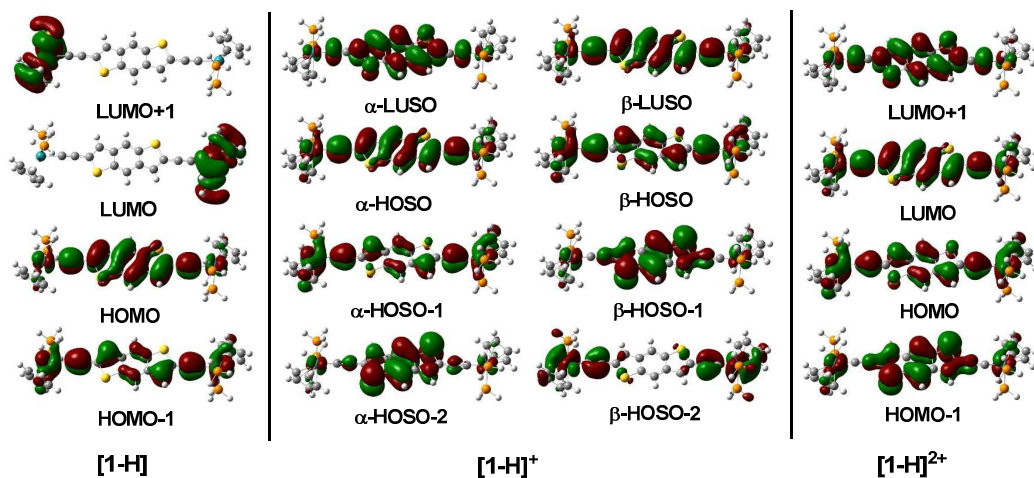


Figure 8. Selected molecular orbitals of model complexes $[1-H]^{n+}$ ($n = 0, 1, 2$) plotted with contour values ± 0.04 (e/bohr^3)^{1/2}

In order to include dynamic behavior of the linear ethynyl-linked bridge in the description of changes in molecular and electronic structures triggered by one-electron oxidation, which were monitored by spectroelectrochemistry, the DFT study was extended with different selected rotamers calculated for non-truncated complexes $[1]^+$ and $[4]^+$, using the global hybrid functional BLYP35 with a suitable continuum solvent model (DCM = dichloromethane). The basis set employed here is 6-31G* (Lan12dz for Ru atom), which has been developed specifically to provide accurate ground- and excited state properties for dinuclear metal mixed-valence systems^[5c, 5d, 10-14, 26c]. According to Kaupp and Low^[11-14], these rotamers typically represent three typical conformations with different fixed P–Ru–Ru–P dihedral angles between the half-sandwich metal terminal groups and the diethynyl-core bridge plane bisecting the two P–Ru–P angles of the diphosphine ligands. The values of the

dihedral angle Ω define three different conformations of the complex, i.e., *cisoid* ($\Omega = 0^\circ$), *perpendicular* ($\Omega = 90^\circ$) and *transoid* ($\Omega = 180^\circ$). Accordingly, monocations $[1]^+$ and $[4]^+$ were also set up artificially into above three forms, viz. *trans*- $[1]^+$, *cis*- $[1]^+$ and *perp*- $[1]^+$ for $[1]^+$ and *trans*- $[4]^+$, *cis*- $[4]^+$ and *perp*- $[4]^+$ for $[4]^+$. Notably, several optimization programs failed in this case to obtain the presumably spin-asymmetric perpendicular conformation of both $[1]^+$ (indicated as a minor component by IR spectroelectrochemistry at room temperature, see above) and $[4]^+$, which may be contributing to their higher-energy structures.

For a deeper insight into the electronic structures of the mono-oxidized states, the BLYP35 DFT calculations were performed on the stable *cisoid* and *transoid* rotamers of monocations $[1]^+$ and $[4]^+$. For symmetric monocation $[1]^+$ showing two $\nu(\text{C}\equiv\text{C})$ bands at 1979 cm^{-1} and 1938 cm^{-1} , the corresponding BLYP35 method gave only a single peak at 2212 cm^{-1} (for both *trans*- $[1]^+$ and *cis*- $[1]^+$). Similarly, calculated *trans*- $[4]^+$ and *cis*- $[4]^+$ rotamers also feature a single intense $\nu(\text{C}\equiv\text{C})$ band at 2169 cm^{-1} and 2171 cm^{-1} (experimental data: 2000 cm^{-1} and 1914 cm^{-1}), respectively. The electronically very similar *trans* and *cis* rotamers exhibit obviously (almost) identical IR $\nu(\text{C}\equiv\text{C})$ absorptions. The DFT calculations have thus succeeded to reproduce the smaller wavenumber of the asymmetric $-\text{C}\equiv\text{C}-\text{core}^+-\text{C}\equiv\text{C}-$ stretching mode for $[4]^+$ compared to $[1]^+$: experiment - $\Delta\tilde{\nu} = 24\text{ cm}^{-1}$, theory - $\Delta\tilde{\nu} = 42\text{ cm}^{-1}$. The appearance of the symmetric $-\text{C}\equiv\text{C}-\text{core}^+-\text{C}\equiv\text{C}-$ stretching mode in the experimental IR spectra of the monocations, not reproduced by the DFT treatment, can be ascribed^[7a] to vibronic coupling with the energetically fairly close-lying MLCT transition, resulting in its enhanced intensity as discussed above in the IR spectroelectrochemistry section.

The B3LYP method chosen for truncated model complexes $[1-\mathbf{H}]^{n+}$ and $[4-\mathbf{H}]^{n+}$ ($n = 0, 1, 2$) served for comparison of the relative $\nu(\text{C}\equiv\text{C})$ shifts caused by oxidation of the neutral parent to monocationic species with the experimental wavenumbers of the asymmetric diethynyl-core stretching mode. Considering the single wavenumber values obtained for $[1-\mathbf{H}]$ (2200 cm^{-1}) and $[1-\mathbf{H}]^+$ (2115 cm^{-1}), and for $[4-\mathbf{H}]$ (2202 cm^{-1}) and $[4-\mathbf{H}]^+$ (2106 cm^{-1}), the calculated values $\Delta\tilde{\nu} = 85\text{ cm}^{-1}$ and 96 cm^{-1} ,

respectively, comply qualitatively with the corresponding experimental data for **1** and **[1]⁺** ($\Delta\tilde{\nu} = 106 \text{ cm}^{-1}$), and for **4** and **[4]⁺** ($\Delta\tilde{\nu} = 129 \text{ cm}^{-1}$).

The delocalized electronic structures calculated with BLYP35 for rotamers *cis/trans*-**[1]⁺** and *cis/trans*-**[4]⁺** are also reflected in the corresponding symmetric distribution of the spin density (Figure 9), delocalized over the molecular backbone including the bridging ligands (the benzodithiophene core and ethynyl linkers) and the metal centers. The contributions concentrate upon the bridging ligands (*trans*-**[1]⁺** : 80%; *cis*-**[1]⁺** : 79%; *trans*-**[4]⁺**: 78%; *cis*-**[4]⁺** : 78%). In addition, merely a subtle difference was found between *trans*-**[4]⁺** and *cis*-**[4]⁺**. The electronic structure of *trans*-**[4]⁺** exhibits only slight asymmetry along the molecular backbone Ru/C \equiv C/BDT/C \equiv C/Ru : 0.10 / 0.13 / 0.50 / 0.15 / 0.12 (BDT = benzodithiophene core).

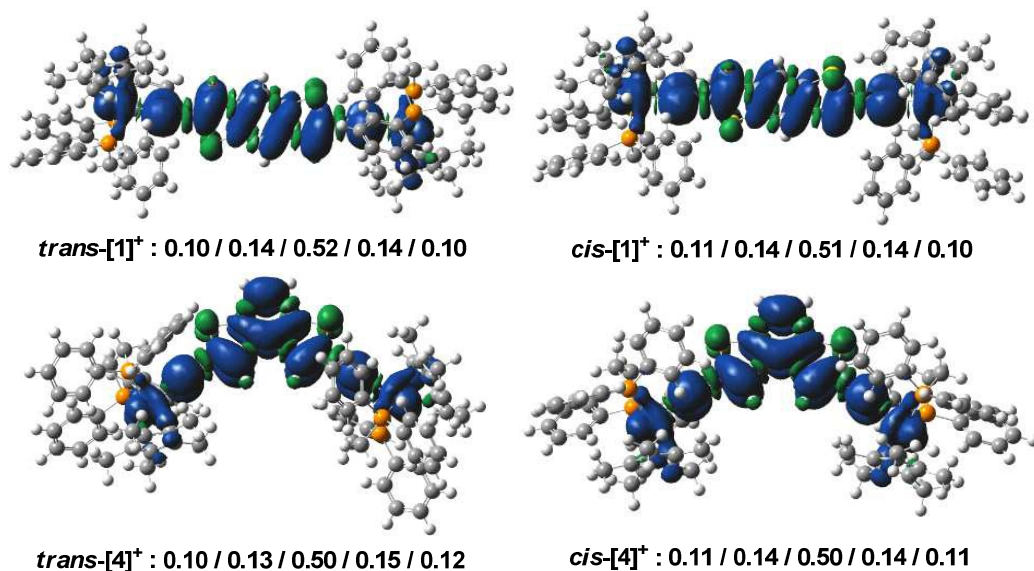


Figure 9. Spin-density distributions in *trans*-**[1]⁺**, *cis*-**[1]⁺** and *trans*-**[4]⁺**, *cis*-**[4]⁺** (Ru/C \equiv C/Ar/C \equiv C/Ru) with the corresponding compositions. Contour values: $\pm 0.04 \text{ (e/bohr}^3)^{1/2}$.

The characteristic NIR electronic absorption of cations **[1]⁺** (Figure 5) and **[4]⁺** (Figure 6) has been well reproduced by TD-DFT calculations (BLYP35). The major electronic excitations in the *transoid* and *cisoid* forms of the non-truncated models of

[1]⁺ and [4]⁺ are listed in Table 6. The corresponding isosurface plots of molecular orbitals involved in the major electronic excitations in [1]⁺ and [4]⁺ are displayed in Figure 10 and Figure S8 (Supporting Information), respectively. The fully optimized structures of [1]⁺ and [4]⁺ exhibit a fairly intense NIR electronic transition near 6350 cm⁻¹ and 4350 cm⁻¹, respectively (*trans*-[1]⁺, 6394 cm⁻¹ ($f = 1.1178$); *cis*-[1]⁺, 6297 cm⁻¹ ($f = 1.1128$); *trans*-[4]⁺, 4318 cm⁻¹ ($f = 0.5211$); *cis*-[4]⁺, 4376 cm⁻¹ ($f = 0.5469$)). Indeed, the calculated NIR maxima are close to the experimental optical absorption energies and the descending trend in wavenumber and intensities is well reproduced, viz. 6000/4540 cm⁻¹ for [1]⁺ and 4300/3200 cm⁻¹ for [4]⁺. The NIR absorption mainly originates from the β -HOSO \rightarrow β -LUSO excitation (Figure 10 and Figure S8), having an obvious mixed ML(bridge)CT and π - π^* (benzodithiophene) character. In addition, the two calculated cationic rotamers feature slightly different absorption wavenumbers, implying that electronic transitions from different conformations are responsible for the broad and structured band envelopes in the NIR region.

According to the TDDFT results (Table 6), multiple absorptions of singly oxidized species **1**⁺ and **4**⁺ in the visible region display similar transition characteristics, being mainly assigned to L'(Cp*, dppe) \rightarrow M and M \rightarrow L(bridge ligand) CT excitations.

Table 6. Major Electronic Excitations of *Transoid* and *Cisoid* Forms of [1]⁺ and [4]⁺ Determined by TD-DFT Methods.

Complex	Conformer	λ /nm [$\tilde{\nu}$ /cm ⁻¹]	Osc. Str. (f)	Major Contributions	Assignment
[1] ⁺	<i>trans</i>	1564 [6394]	1.1178	β -HOSO \rightarrow β -LUSO (98%)	ML(bridge ligand)CT π - π^* (benzodithiophene)
		537 [18622]	0.1905	β -HOSO-7 \rightarrow β -LUSO (84%)	L'(Cp*, dppe)MCT ML(bridging)CT
	<i>cis</i>	508 [19685]	0.8284	α -HOSO \rightarrow α -LUSO (74%)	ML(bridge ligand)CT π - π^* (benzodithiophene)
		1588 [6297]	1.1128	β -HOSO \rightarrow β -LUSO (98%)	ML(bridge ligand)CT π - π^* (benzodithiophene)

	958 [10438]	0.0024	β -HOSO-2 \rightarrow β -LUSO (64%)	L'(Cp*, dppe)MCT ML(bridge ligand)CT
	538 [18587]	0.1564	β -HOSO-7 \rightarrow β -LUSO (85%)	MLCT/L'(Cp*)MCT
	509 [19646]	0.8461	α -HOSO \rightarrow α -LUSO (75%)	ML(bridge ligand)CT π - π^* (benzodithiophene)
	2316 [4318]	0.5211	β -HOSO \rightarrow β -LUSO (99%)	MLCT π - π^* (benzodithiophene)
<i>trans</i>	767 [13038]	0.0441	β -HOSO-3 \rightarrow β -LUSO (81%)	MLCT/ILCT
	653 [15314]	0.1588	β -HOSO-7 \rightarrow β -LUSO (60%)	MLCT
	493 [20284]	0.4390	α -HOSO \rightarrow α -LUSO (78%)	ML(bridge ligand)CT π - π^* (benzodithiophene)
[4] ⁺	2285 [4376]	0.5469	β -HOSO \rightarrow β -LUSO (99%)	MLCT π - π^* (benzodithiophene)
	750 [13333]	0.0760	β -HOSO-3 \rightarrow β -LUSO (97%)	MLCT/L'(Cp*)MCT
<i>cis</i>	647 [15456]	0.1517	β -HOSO-6 \rightarrow β -LUSO (74%)	ML(bridge ligand)CT L'(Cp*)MCT
	494 [20243]	0.4870	α -HOSO \rightarrow α -LUSO (81%)	MLCT π - π^* (benzodithiophene)

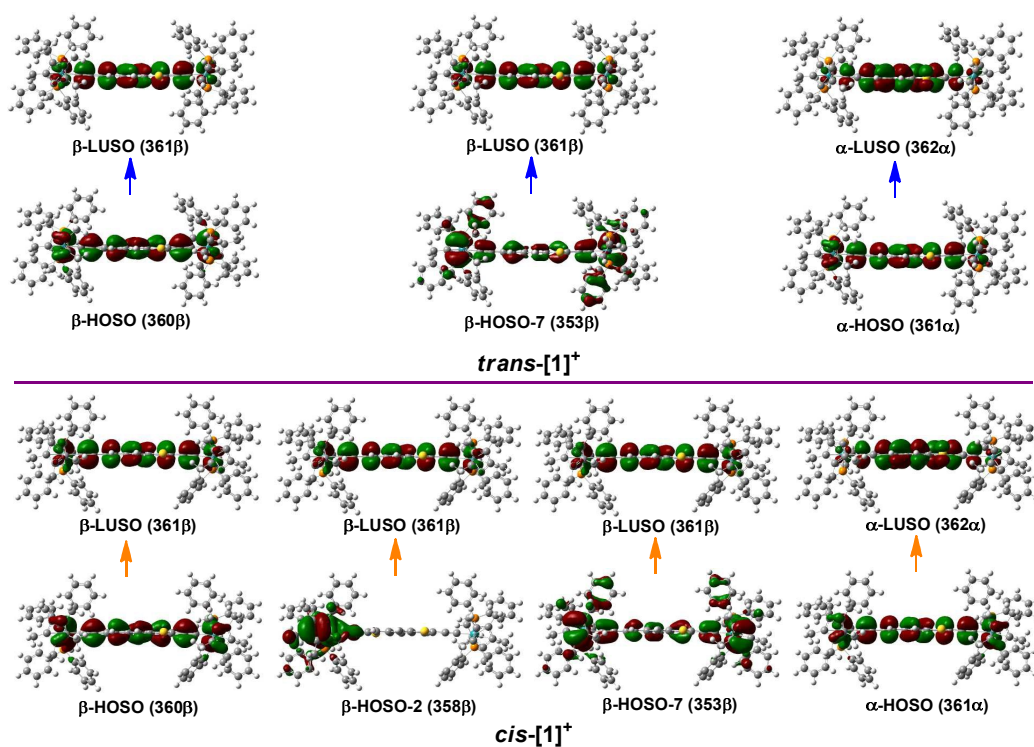


Figure 10. Isosurface plots of molecular orbitals involved in the major electronic excitations in *trans*-[1]⁺ and *cis*-[1]⁺

Conclusions

The studied diruthenium complexes featuring different linear (**1** and **2**) and bent (**3** and **4**) benzodithiophene isomers in the core of the ethynyl-terminated bridging ligands exhibit oxidation largely localized on the bridging ligands, with a dominant contribution from the benzodithiophene core. The first two anodic steps of complexes **1**, **3** and **4** are well defined at ambient temperature whereas the oxidation of **2** is totally irreversible. Only complexes **1** and **4** form stable cations and dication suited for spectroelectrochemical studies. The monocations in their *transoid* and *cisoid* conformations show composed absorption bands in the NIR region assigned to bridge π - π^* and MLCT transitions. The heavy involvement of the isomeric benzodithiophene core is indicated by the observed differences in energies and intensities of the NIR absorption maxima, in agreement with results of TDDFT (BLYP35) calculations that reproduce appreciably the experimental features. The symmetric distribution of the

spin density dominantly over the non-innocent bridging ligand follows from the DFT description of the bonding situation in the dominant conformations of $[1]^+$ and $[4]^+$. The former linear cation may also co-exist in another, less stable thermally populated conformation (rotamer) with asymmetric spin density distribution due to localized oxidation (a mixed valence species), as testified by IR spectroelectrochemistry at variable temperature. Two-electron-oxidized $[1]^{2+}$ and $[4]^{2+}$ exhibit the characteristic MLCT/ π - π^* electronic absorption shifted to the red spectral region. Vibronic coupling of the low-energy charge transfer transitions with the $\nu(\text{C}\equiv\text{C})$ vibrations of the ethynyl linkers is the likely reason for the observed two $\nu(\text{C}\equiv\text{C})$ bands in the IR spectra of both the monocations and dication in their electronically very similar *cisoid* and *transoid* conformations, the symmetric stretching mode of the $-\text{C}\equiv\text{C}-\text{core}^{n+}-\text{C}\equiv\text{C}-$ unit being significantly enhanced in intensity compared to the neutral precursors. The attachment of the redox active $\text{Cp}^*\text{Ru}(\text{dppe})$ terminal groups provides an excellent opportunity to compare diethynyl-linked bridging ligands featuring different cores used to tune the extent of electronic communication between the Ru-ethynyl groups. In this regard trends in redox and spectroscopic properties (e.g., oxidation potentials, low-energy electronic absorption, $\nu(\text{C}\equiv\text{C})$ wavenumbers) observed for complexes $[1]^{n+}$ and $[4]^{n+}$ ($n = 0, 1, 2$) strongly resemble those previously reported^[7b] for congeners with diethynyl bi- and terthiophene bridges, respectively. This conclusion underlines the general importance of studying redox active molecular bridges featuring isomeric forms of the same non-innocent core component.

Experimental

General Materials. All manipulations were carried out under an argon atmosphere by using standard Schlenk techniques, unless otherwise stated. Solvents were pre-dried, distilled, and degassed prior to use, except those for spectroscopic measurements, which were of spectroscopic grade. Trimethylsilyl acetylene (TMSA) and KF were commercially available and used without further purification. The starting materials

[Cp*RuCl(dppe)]^[29], 2,6-dibromobenzo[1,2-b:4,5-b']dithiophene (**1a**), 2,6-dibromobenzo[1,2-b:5,4-b']dithiophene (**2a**), 2,7-dibromobenzo[1,2-b:3,4-b']dithiophene (**3a**), 2,7-dibromobenzo[1,2-b:4,3-b']dithiophene (**4a**), were prepared by procedures described in the literature^[30-33].

Synthesis of Bis((trimethylsilyl)ethynyl)benzodithiophene (**1b - 4b**)^[25]

2,6-Bis(trimethylsilylethynyl)benzo[1,2-b:4,5-b']dithiophene (**1b**). To a stirred solution of 2,6-dibromobenzo[1,2-b:4,5-b']dithiophene **1a** (200 mg, 0.58 mmol), CuI (11 mg, 0.058 mmol), and [Pd(PPh₃)₄] (67 mg, 0.058 mmol) in triethylamine (12 mL) and THF (12 mL) under an argon atmosphere TMSA (282 mg, 2.88 mmol) was added and the mixture was refluxed for 24 h. The cold solution was filtered through a bed of celite. The filtrate was evaporated under reduced pressure and purified by silica gel column chromatography (petroleum ether) to give a light yellow solid (100 mg, 0.26 mmol, 45%). ¹H NMR (400 MHz, CDCl₃): δ 0.28 (s, 18H, SiMe₃), 7.46 (s, 2H), 8.08 (s, 2H). ¹³C NMR (100 MHz, CDCl₃): δ -0.23, 97.7, 101.9, 116.5, 124.0, 128.5, 129.1, 137.6. Anal. Calcd for C₂₀H₂₂S₂Si₂: C, 62.77; H, 5.79. Found: C, 62.69; H, 5.85.

2,6-Bis(trimethylsilylethynyl)benzo[1,2-b:5,4-b']dithiophene (**2b**) The preparative procedure of **2b** was similar to that for **1b**. Amounts of reagents: **2a** (400 mg, 1.16 mmol), CuI (22 mg, 0.116 mmol), [Pd(PPh₃)₄] (134 mg, 0.116 mmol), triethylamine (25 mL) and THF (25 mL), TMSA (564 mg, 5.76 mmol). Yield: 300 mg, 0.78 mmol (68%) of a white solid. ¹H NMR (400 MHz, CDCl₃): δ 0.28 (s, 18H, SiMe₃), 7.46 (s, 2H), 8.02 (s, 1H), 8.06 (s, 1H). ¹³C NMR (100 MHz, CDCl₃): δ -0.22, 97.6, 101.6, 114.6, 118.2, 123.0, 129.1, 137.1, 138.5. Anal. Calcd for C₂₀H₂₂S₂Si₂: C, 62.77; H, 5.79. Found: C, 62.86; H, 5.70.

2,7-Bis(trimethylsilylethynyl)benzo[1,2-b:3,4-b']dithiophene (**3b**) The preparative procedure of **3b** was similar to that for **1b**. Amounts of reagents: **3a** (225 mg, 0.65 mmol), CuI (12 mg, 0.065 mmol), [Pd(PPh₃)₄] (75 mg, 0.065 mmol), diisopropylamine (20 mL) and THF (20 mL), TMSA (254 mg, 2.59 mmol). Yield: 173 mg, 0.45 mmol (70%) of a white solid. ¹H NMR (400 MHz, CDCl₃): δ 0.31 (s, 18H, SiMe₃), 7.54 (s, 1H), 7.63 (s, 1H), 7.68 (s, 2H). ¹³C NMR (100 MHz, CDCl₃): δ

-0.2, 97.3, 97.6, 100.9, 101.9, 118.9, 121.4, 121.7, 124.30, 126.7, 130.1, 132.3, 134.8, 136.3, 137.8. Anal. Calcd for $C_{20}H_{22}S_2Si_2$: C, 62.77; H, 5.79. Found: C, 62.82; H, 5.69.

2,7-Bis(trimethylsilylethynyl)benzo[1,2-b:4,3-b']dithiophene (**4b**) The preparative procedure of **4b** was similar to that for **1b**. Amounts of reagents: **4a** (200 mg, 0.58 mmol), CuI (11 mg, 0.058 mmol), $[Pd(PPh_3)_4]$ (67 mg, 0.058 mmol), diisopropylamine (20 mL) and THF (20 mL), TMSA (225 mg, 2.30 mmol). Yield: 187 mg, 0.49 mmol (85%) of a white solid. 1H NMR (400 MHz, $CDCl_3$): δ 0.29 (s, 18H, SiMe₃), 7.70 (s, 2H), 7.75 (s, 2H). ^{13}C NMR (100 MHz, $CDCl_3$): δ -0.2, 97.6, 101.7, 119.5, 123.8, 127.2, 133.7, 137.3. Anal. Calcd for $C_{20}H_{22}S_2Si_2$: C, 62.77; H, 5.79. Found: C, 62.69; H, 5.83.

General Synthesis of Binuclear Ruthenium Complexes **1** - **4**^[34]

Preparation of **1**. A solution of $[Cp^*RuCl(dppe)]$ (258 mg, 0.38 mmol), 2,6-bis(trimethylsilylethynyl)benzo[1,2-b:4,5-b']dithiophene (**1b**) (70 mg, 0.14 mmol), and KF (127 mg, 2.20 mmol) in CH_3OH (20 mL) and THF (4 mL) was heated to reflux under nitrogen atmosphere for 24 h. The crude product was collected by filtration, washed with methanol (10 mL) and hexane (10 mL), The solid was dissolved in dichloromethane and precipitated from slow diffusion with hexane. The solid was filtered and dried to give **1** as a deep yellow powder (180 mg, 0.11 mmol, 64%). 1H NMR (400 MHz, $CDCl_3$): δ 1.56 (s, 30H, $2C_5(CH_3)_5$), 2.07 (br, 4H, $CH_2/dppe$), 2.69 (br, 4H, $CH_2/dppe$), 6.43 (s, 2H), 7.20-7.38 (m, 32H, $H_{Ar/dppe}$), 7.60 (s, 2H), 7.76 (br, 8H, $H_{Ar/dppe}$). ^{13}C NMR (100 MHz, $CDCl_3$): δ 10.0 (CH_3), 29.5 (t, $J = 22.90$ Hz, $CH_2/dppe$), 93.0 (CH/C_5Me_5), 103.4 (thiophene-C \equiv C), 113.3 (Ru-C \equiv C), 119.0, 127.4, 129.0, 130.3, 133.22, 133.6, 135.8, 136.4, 136.9, 137.7, 138.4, 138.7, 142.4. ^{31}P NMR (160 MHz, $CDCl_3$): δ 79.1 (dppe). IR (KBr/ cm^{-1}): $\nu(C\equiv C)$ 2054 (w). Anal. Calcd for $C_{86}H_{81}P_4Ru_2S_2$: C, 68.64; H, 5.43. Found: C, 68.80; H, 5.31.

Preparation of **2**. The synthetic procedure employed for **2** was similar to that for **1**. Amounts of reagents: $[Cp^*RuCl(dppe)]$ (275 mg, 0.41 mmol),

2,6-bis(trimethylsilylethynyl)benzo[1,2-b:5,4-b']dithiophene (**2b**) (70 mg, 0.14 mmol) and KF (127 mg, 2.20 mmol) in CH₃OH (20 mL) and THF (5 mL). Yield: 160 mg, 0.10 mmol (57%) of a yellow solid. ¹H NMR (400 MHz, CDCl₃): δ 1.56 (s, 30H, 2C₅(CH₃)₅), 2.07 (br, 4H, CH₂/dppe), 2.69 (br, 4H, CH₂/dppe), 6.46 (s, 2H), 7.20-7.38 (m, 32H, H_{Ar}/dppe), 7.54 (s, 1H), 7.67 (s, 1H), 7.77 (br, 8H, H_{Ar}/dppe). ¹³C NMR (100 MHz, CDCl₃): δ 10.0 (CH₃), 29.5 (t, *J* = 22.80 Hz, CH₂/dppe), 93.0 (CH/C₅Me₅), 103.0 (s, thiophene-C≡C), 113.3(Ru-C≡C), 119.4, 127.4, 129.0, 130.4, 133.2, 133.6, 134.8, 136.4, 136.7, 136.9, 138.4, 138.6, 138.7, 141.9. ³¹P NMR (160 MHz, CDCl₃): δ 79.2 (dppe). IR (KBr/cm⁻¹): ν(C≡C) 2049 (w). Anal. Calcd for C₈₆H₈₁P₄Ru₂S₂: C, 68.64; H, 5.43. Found: C, 68.91; H, 5.22.

Preparation of **3**. The synthetic procedure employed for **3** was similar to that for **1**. Amounts of reagents: [Cp*RuCl(dppe)] (331 mg, 0.50 mmol), 2,7-bis(trimethylsilylethynyl)benzo[1,2-b:3,4-b']dithiophene (**3b**) (90 mg, 0.23 mmol) and KF (163 mg, 2.97 mmol) in CH₃OH (20 mL) and THF (5 mL). Yield: 170 mg, 0.11 mmol (48%) of a deep yellow solid. ¹H NMR (400 MHz, CDCl₃): δ 1.58 (s, 30H, 2C₅(CH₃)₅), 2.08 (br, 4H, CH₂/dppe), 2.72 (br, 4H, CH₂/dppe), 6.49(s, 1H), 6.51(s, 1H), 7.26-7.31(m, 32H+2H, H_{Ar}/dppe+H_{benzothiophene}), 7.77 (br, 8H, H_{Ar}/dppe). ¹³C NMR (100 MHz, CDCl₃): δ 10.0(CH₃), 29.4 (t, *J* = 22.9 Hz, CH₂/dppe), 92.9 (CH/C₅Me₅), 102.4 (thiophene-C≡C), 102.8 (thiophene-C≡C), 117.0, 117.4, 117.8, 120.4 (Ru-C≡C), 127.4, 128.9, 129.0, 129.9, 130.4, 132.3, 133.2, 133.6, 133.6, 133.8, 136.3, 136.5, 136.8, 136.9, 137.2, 138.3, 138.7, 140.0, 142.9. ³¹P NMR (160 MHz, CDCl₃): δ 79.9 (dppe). IR (KBr/cm⁻¹): ν(C≡C) 2049 (w). Anal. Calcd for C₈₆H₈₂P₄Ru₂S₂: C, 68.60; H, 5.49. Found: C, 68.77; H, 5.29.

Preparation of **4**. The synthetic procedure employed for **4** was similar to that for **1**. Amounts of reagents: [Cp*RuCl(dppe)] (368 mg, 0.55 mmol), 2,7-bis(trimethylsilylethynyl)benzo[1,2-b:4,3-b']dithiophene (**4b**) (100 mg, 0.26 mmol) and KF (181 mg, 3.30 mmol) in CH₃OH (20 mL) and THF (5 mL). Yield: 150 mg, 0.09 mmol (38%) of a deep yellow solid. ¹H NMR (400 MHz, CDCl₃): δ 1.58 (s, 30H, 2C₅(CH₃)₅), 2.09 (br, 4H, CH₂/dppe), 2.72 (br, 4H, CH₂/dppe), 6.66 (s, 2H), 7.01(d,

$J(\text{HH}) = 7.2$ Hz, 2H, Ar), 7.30-7.40 (m, 32H, $\text{H}_{\text{Ar/dppe}}$), 7.79 (br, 8H, $\text{H}_{\text{Ar/dppe}}$). ^{13}C NMR (100 MHz, CDCl_3): δ 10.0 (CH_3), 29.7 (t, $J = 22.90$ Hz, CH_2/dppe), 92.9 ($\text{CH}/\text{C}_5\text{Me}_5$), 102.9 (s, thiophene- $\text{C}\equiv\text{C}$), 116.1 ($\text{Ru}-\text{C}\equiv\text{C}$), 118.6, 127.4, 129.0, 131.4, 133.2, 133.6, 134.1, 136.4, 136.9, 138.3, 141.9. ^{31}P NMR (160 MHz, CDCl_3): δ 79.9 (dppe). IR ($\text{KBr}/\text{cm}^{-1}$): $\nu(\text{C}\equiv\text{C})$ 2050 (w). Anal. Calcd for $\text{C}_{86}\text{H}_{82}\text{P}_4\text{Ru}_2\text{S}_2$: C, 68.60; H, 5.49. Found: C, 68.71; H, 5.35.

Crystallographic Details. Single crystals of $1 \cdot 4/3 \text{CH}_2\text{Cl}_2 \cdot 3/2$ toluene, **2** and $3 \cdot 1/4 \text{CH}_2\text{Cl}_2$ were obtained by slow diffusion of hexane into a dichloromethane solution of containing **1**, **2** and **3** at room temperature, respectively. The toluene molecule in the crystal of **1** comes from a post-reaction treatment. Crystals with approximate dimensions of $0.23 \times 0.20 \times 0.02 \text{ mm}^3$ for **1**, $0.16 \times 0.12 \times 0.10 \text{ mm}^3$ for **2** and $0.16 \times 0.12 \times 0.10 \text{ mm}^3$ for **3** were mounted on glass fibers for diffraction experiments. Intensity data were collected on a Nonius Kappa CCD diffractometer with Mo $\text{K}\alpha$ radiation (0.71073 \AA) at room temperature. The molecular structures were solved by a combination of direct methods (SHELXS-97)^[35] and Fourier difference techniques and refined by fullmatrix least squares (SHELXL-97)^[36]. All non-H atoms were refined anisotropically. The hydrogen atoms were placed in ideal positions and refined as riding atoms. The partial solvent molecules have been omitted. Further crystal data and details of the data collection are summarized in Table S1. Selected bond distances and angles are given in Table 1, respectively.

Physical Measurements. ^1H , ^{13}C , and ^{31}P NMR spectra were collected on a Varian Mercury Plus 400 spectrometer (400 MHz) operating at 298 K in the Fourier transform mode. ^1H and ^{13}C NMR chemical shifts are relative to TMS, and ^{31}P NMR chemical shifts are relative to 85% H_3PO_4 , which are reported in δ (parts per million). Elemental analyses (C, H, N) were performed with a Vario EIII Chnso instrument. The voltammetric measurements were performed on a CHI 660C potentiostat (CHI USA). A three-electrode single-compartment cell was used for the solution of complexes and supporting electrolyte in dry CH_2Cl_2 . The solution was deaerated by

argon bubbling on a frit for about 10 min before the measurement. The analyte (complex, ligand) and electrolyte (Bu_4NPF_6) concentrations were typically 10^{-3} and 10^{-1} mol dm^{-3} , respectively. A pre-polished 500- μm diameter platinum disk working electrode, a platinum wire counter electrode, and an Ag/Ag^+ reference electrode were used. Spectroelectrochemical experiments at room temperature were performed with an airtight optically transparent thin-layer electrochemical (OTTLE) cell (optical path length of ca 200 μm) equipped with a Pt minigrid working electrode and CaF_2 windows.^[37a] The cell was positioned in the sample compartment of a Bruker Tensor FT-IR spectrometer (1 cm^{-1} spectral resolution, 8 scans), Bruker Vertex 70v FT-IR spectrometer (1 cm^{-1} spectral resolution, 16 scans) or a Shimadzu UV-3600 UV-Vis-NIR spectrophotometer. The controlled-potential electrolyses were carried out with a CHI 660C potentiostat. The concentration of samples was ca 2×10^{-3} mol dm^{-3} . Dry 10^{-1} M Bu_4NPF_6 was used as the supporting electrolyte. The IR-NIR spectroelectrochemistry at 223 K (dichloromethane, 3×10^{-1} M Bu_4NPF_6) was conducted with a cryostatted version of the OTTLE cell^[37b] equipped with CaF_2 optical windows and positioned in the sample compartment of a Bio-Rad MCT detector module linked to a Bruker Vertex 70v FT-IR spectrometer. The potential control was achieved with an EmStat3+ potentiostat (PalmSens, The Netherlands).

Computational Details. Density functional theory (DFT) calculations were performed using the Gaussian09 software^[38], at the B3LYP/3-21G* and BLYP35^[14]/6-31G* levels of theory. Geometry optimizations and full Geometry optimizations were performed without any symmetry constraints, and frequency calculations on the resulting optimized geometries showed no imaginary frequencies. Electronic transitions were calculated by the time-dependent DFT (TD-DFT) method. The MO contributions were generated using the Multiwfn2.6.1_bin_Win package and plotted using GaussView 5.0. The solvation effects in dichloromethane are included for a part of the calculations with the conductor-like polarizable continuum model (CPCM)^[39].

Acknowledgements

The authors acknowledge financial support from National Natural Science Foundation of China (21272088, 21472059, 21402057), the Opening Subjects of Hunan Province Key Laboratory of Functional Organometallic Materials (No. GN15K05), the Scientific Research Foundation of Hengyang Normal University (No. 14B23), Scientific Research Project of Education Department of Hunan Province (No. 14C0168). F.H. thanks the University of Reading for the support of the Reading Spectroelectrochemistry laboratory (Project D14-015).

Author Information

Corresponding Authors

*E-mail: chshliu@mail.ccnu.edu.cn (S.H.L.); f.hartl@reading.ac.uk (F. H.).

Notes

The authors declare no competing financial interests.

† **Electronic supplementary information (ESI) available:** IR and UV-Vis-NIR spectroelectrochemistry, calculated DFT data, and NMR information. CCDC number 1429882 & 1429879 & 1430066 for **1**, **2** and **3**. ESI and crystallographic data in CIF or other electronic format are available free of charge via the Internet at <http://pubs.acs.org>.

References

- [1] (a) Karmakar, S.; Maity, D.; Mardanya, S.; Baitalik, S. *Inorg. Chem.*, **2014**, *53*, 12036-12049. (b) Xu, P.; Wu, H.; Xia, H.; Ye, S.; Du, P. *Organometallics*, **2014**, *33*, 2738-2746. (c) McCall, K. L.; Jennings, G. R.; Wang, H.; Morandeira, A.; Peter, L. M.; Durrant, J. R.; Yellowlees, L. J.; Robertson, N. *Eur. J. Inorg. Chem.* **2011**, 589-596. (d) Carlson, C. N.; Scott, B. L.; Martin, R. L.; Thompson, J. D.; Morris, D. E.; John, K. D. *Inorg. Chem.*, **2007**, *46*, 5013-5022. (e) Brunschwig, B. S.; Creutz, C.; Sutin, N. *Chem. Soc. Rev.* **2002**, *31*, 168-184.
- [2] (a) Wen, H.-M.; Yang, Y.; Liu, J.-Y.; Zhang, D.-B.; Chen, Z.-B.; Wang, J.-Y.;

- Chen, Z.-N.; Tian, Z.-Q. *Chem. Sci.*, **2013**, *4*, 2471-2477. (b) Launay, J.-P. *Coord. Chem. Rev.*, **2013**, *257*, 1544-1554. (c) Aguirre-Etcheverry, P.; O'Hare, D. *Chem. Rev.* **2010**, *110*, 4839-4864. (d) Xu, G.-L.; Zou, G.; Ni, Y.-H.; DeRosa, M. C.; Crutchley, R. J.; Ren, T. *J. Am. Chem. Soc.* **2003**, *125*, 10057-10065. (e) Yao, C.-J.; Zhong, Y.-W.; Yao, J. *J. Am. Chem. Soc.* **2011**, *133*, 15697-15706. (f) Linseis, M.; Záliš, S.; Zabel, M.; Winter, R. F. *J. Am. Chem. Soc.* **2012**, *134*, 16671-16692. (g) Liu, S. H.; Xia, H.; Wen, T. B.; Zhou, Z. Y.; Jia, G. *Organometallics* **2003**, *22*, 737-743. (h) Hildebrandt, A.; Lang, H. *Organometallics* **2013**, *32*, 5640-5653.
- [3] (a) Costuas, K.; Rigaut, S. *Dalton Trans.*, **2011**, *40*, 5643-5658. (b) Ceccon, A.; Santi, S.; Orian, L.; Bisello, A. *Coord. Chem. Rev.* **2004**, *248*, 683-724.
- [4] (a) Brunschwig, B. S.; Creutz, C.; Sutin, N. *Chem. Soc. Rev.*, **2002**, *31*, 168-184. (b) Tuccitto, N.; Ferri, V.; Cavazzini, M.; Quici, S.; Zhavnerko, G.; Licciardello, A.; Rampi, M. A. *Nat. Mater.* **2008**, *8*, 41-46. (c) Li, F.; Basile, V. M.; Rose, M. J. *Langmuir*, **2015**, *31*, pp 7712-7716.
- [5] (a) Lapinte, C. *J. Organomet. Chem.* **2008**, *693*, 793-801. (b) Lu, Y.; Quardokus, R.; Lent, C. S.; Justaud, F.; Lapinte, C.; Alex Kandel, S. *J. Am. Chem. Soc.* **2010**, *132*, 13519-13524. (c) Makhoul, R.; Sahnoune, H.; Dorcet, V.; Halet, J.-F.; Hamon, J.-R.; Lapinte, C. *Organometallics*, **2015**, *34*, 3314-3326. (d) Pfaff, U.; Hildebrandt, A.; Korb, M.; Schaarschmidt, D.; Rosenkranz, M.; Popov, A.; Lang, H. *Organometallics*, **2015**, *34*, 2826-2840.
- [6] (a) Shah, H. H.; Al-Balushi, R. A.; Al-Suti, M. K.; Khan, M. S.; Woodall, C. H.; Molloy, K. C.; Raithby, P. R.; Robinson, T. P.; Dale, S. E. C.; Marken, F. *Inorg. Chem.*, **2013**, *52*, 4898-4908. (b) Engrakul, C.; Sita, L. R. *Organometallics* **2008**, *27*, 927-937.
- [7] (a) Fox, M. A.; Guennic, B. L.; Roberts, R. L.; Brue, D. A.; Yufit, D. S.; Howard, J. A. K.; Manca, G.; Halet, J.-F.; Hartl, F.; Low, P. J. *J. Am. Chem. Soc.* **2011**, *133*, 18433-18446. (b) Ou, Y.-P.; Xia, J.; Zhang, J.; Xu, M.; Yin, J.; Yu, G.-A.; Liu, S. H. *Chem. Asian J.* **2013**, *8*, 2023-2032. (c) Zhang, J.; Ou, Y.-P.; Xu, M.; Sun, C.; Yin,

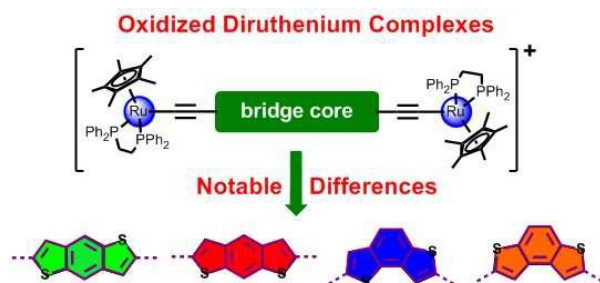
- J.; Yu, G.-A.; Liu, S. -H. *Eur. J. Inorg. Chem.* **2014**, 2941-2951.
- [8] Fox, M. A.; Farmer, J. D.; Roberts, R. L.; Humphrey, M. G.; Low, P. J. *Organometallics* **2009**, *28*, 5266-5269.
- [9] Klein, A.; Lavastre, O.; Fiedler, J. *Organometallics* **2006**, *25*, 635-643.
- [10] Burgun, A.; Gendron, F.; Sumby, C.; Roisnel, T.; Cador, O.; Costuas, K.; Halet, J.-F.; Bruce, M. I.; Lapinte, C. *Organometallics* **2014**, *33*, 2613-2627.
- [11] Parthey, M.; Gluyasz, J. B. G.; Schauer, P. A.; Yufit, D. S.; Howard, J. A. K.; Kaupp, M.; Low, P. J. *Chem. Eur. J.* **2013**, *19*, 9780-9784.
- [12] Parthey, M.; Gluyas, J. B. G.; Fox, M. A.; Low, P. J.; Kaupp, M. *Chem. Eur. J.* **2014**, *20*, 6895-6908.
- [13] Marqués-González, S.; Parthey, M.; Yufit, D. S.; Howard, J. A. K.; Kaupp, M.; Low, P. J. *Organometallics* **2014**, *33*, 4947-4963.
- [14] (a) Parthey, M.; Kaupp, M. *Chem. Soc. Rev.*, **2014**, *43*, 5067-5088. (b) Renz, M., Theilacker, K., Lambert, C., Kaupp, M. *J. Am. Chem. Soc.* **2009**, *131*, 16292-16302. (c) Kaupp, M., Renz, M., Parthey, M., Stolte, M., Würthner, F., Lambert, C. *Phys. Chem. Chem. Phys.* **2011**, *13*, 16973-16986.
- [15] Takimiya, K.; Osaka, I.; Mori, T.; Nakano, M. *Acc. Chem. Res.*, **2014**, *47*, 1493-1502.
- [16] Cinar, M. E.; Ozturk, T. *Chem. Rev.*, **2015**, *115*, 3036-3140.
- [17] Kraft, U.; Anthony, J. E.; Ripaud, E.; Loth, M. A.; Weber, E.; Klauk, H. *Chem. Mater.*, **2015**, *27*, 998-1004.
- [18] Kang, T. E.; Kim, T.; Wang, C.; Yoo, S. and Kim, B. *Chem. Mater.*, **2015**, *27*, 2653-2658.
- [19] Rieger, R.; Beckmann, D.; Mavrinskiy, A.; Kastler, M.; Müllen, K. *Chem. Mater.* **2010**, *22*, 5314-5318.
- [20] Muraoka, K.; Watanabe, Y.; Takahashi, A.; Kamoto, H.; Ogawa, S. *Heteroat. Chem.* **2014**, *25*, 473-481.
- [21] CCDC 1429882 (1), 1429879 (2) and 1430066 (3) contain the supplementary crystallographic data for this paper. These data can be obtained free of charge

from The Cambridge Crystallographic Data Centre via www.ccdc.cam.ac.uk/data_request/cif.

- [22] (a) Fox, M. A.; Roberts, R. L.; Baines, T. E.; Guennic, B. L.; Halet, J. F.; Hartl, F.; Yufit, D. S.; Albesa-Jové, D.; Howard, J. A. K.; Low, P. J. *J. Am. Chem. Soc.* **2008**, *130*, 3566-3578. (b) D'Alessandro, D. M.; Keene, F. R. *Dalton Trans.*, **2004**, 3950-3954.
- [23] Fox, M. A.; Farmer, J. D.; Roberts, R. L.; Humphrey, M. G.; Low, P. J. *Organometallics* **2009**, *28*, 5266-5269.
- [24] Vilà, N.; Zhong, Y.-W.; Henderson, J. C.; Abruña, H. D. *Inorg. Chem.* **2010**, *49*, 796-804.
- [25] Ou, Y.-P.; Jiang, C.; Wu, D.; Xia, J.; Yin, J.; Jin, S.; Yu, G.-A.; Liu, S. H. *Organometallics* **2011**, *30*, 5763-5770.
- [26] (a) Maurer, J.; Sarkar; Schwederski, B.; Kaim, W.; Winter, R. F.; Zálíš, S. *Organometallics* **2006**, *25*, 3701-3712. (b) Polit, W.; Mück, P.; Wuttke, E.; Exner, T.; Winter, R. F. *Organometallics* **2013**, *32*, 5461-5472. (c) Zhang, J.; Zhang, M.-X.; Sun, C.-F.; Xu, M.; Hartl, F.; Yin, J.; Yu, G.-A.; Rao, L.; Liu, S. H. *Organometallics* **2015**, *34*, 3967-3978.
- [27] (a) Gao, L.-B.; Kan, J.; Fan, Y.; Zhang, L.-Y.; Liu, S. H.; Chen, Z.-N. *Inorg Chem.* **2007**, *46*, 5651-5664. (b) Lambert, C.; Amthor, S.; Schelter, J. *J. Phys. Chem. A* **2004**, *108*, 6474-6486.
- [28] Liu, A.; Sauer, M. C., Jr.; Loffredo, D. M.; Trifunac, A. D. *J. Photochem. Photobiol. A* **1992**, *67*, 197-200.
- [29] Bruce, M. I., Ellis, B. G., Low, P. J., Skelton, B. W., White, A. H., *Organometallics*, **2003**, *22*, 3184-3198.
- [30] Rieger, R.; Beckmann, D.; Mavrinskiy, A.; Kastler, M.; Müllen, K. *Chem. Mater.*, **2010**, *22*, 5314-5318.
- [31] Wang, Y.; Parkin, S. R.; Watson, M. D. *Org. Lett.*, **2008**, *10*, 4421-4424.
- [32] Hart, H.; Harada, K.; Du, C. J. F. *J. Org. Chem.*, **1985**, *50*, 3104-3110.
- [33] Archer, W. J.; Cook, R.; Taylor, R. *J. Chem. Soc. Perkin Trans II.*, **1983**,

- 813-819.
- [34] Xia, J.-L.; Man, W.-Y.; Zhu, X.-X.; Zhang, C.; Jin, G.-J.; Schauer, P. A.; Fox, M. A.; Yin, J.; Yu, G.-A.; Low, P. J.; Liu, S. H. *Organometallics* **2012**, *31*, 5321-5333.
- [35] Sheldrick, G. M. SHELXS-97, a Program for Crystal Structure Solution; University of Göttingen: Göttingen, Germany, **1997**.
- [36] Sheldrick, G. M. SHELXL-97, a Program for Crystal Structure Refinement; University of Göttingen, Göttingen, Germany, **1997**.
- [37] (a) Krejčík, M.; Daněk, M.; Hartl, F. *J. Electroanal. Chem. Interfacial Electrochem.* **1991**, *317*, 179-187. (b) Mahabiersing, T.; Luyten, H.; Nieuwendam, R. C.; Hartl, F. *Coll. Czech. Chem. Commun.* **2003**, *68*, 1687-1709.
- [38] Gaussian 09, Revision D.01, Frisch, M. J.; Trucks, G. W.; Schlegel, H. B.; Scuseria, G. E.; Robb, M. A.; Cheeseman, J. R.; Scalmani, G.; Barone, V.; Mennucci, B.; Petersson, G. A.; Nakatsuji, H.; Caricato, M.; Li, X.; Hratchian, H. P.; Izmaylov, A. F.; Bloino, J.; Zheng, G.; Sonnenberg, J. L.; Hada, M.; Ehara, M.; Toyota, K.; Fukuda, R.; Hasegawa, J.; Ishida, M.; Nakajima, T.; Honda, Y.; Kitao, O.; Nakai, H.; Vreven, T.; Montgomery, J. A., Jr.; Peralta, J. E.; Ogliaro, F.; Bearpark, M.; Heyd, J. J.; Brothers, E.; Kudin, K. N.; Staroverov, V. N.; Kobayashi, R.; Normand, J.; Raghavachari, K.; Rendell, A.; Burant, J. C.; Iyengar, S. S.; Tomasi, J.; Cossi, M.; Rega, N.; Millam, J. M.; Klene, M.; Knox, J. E.; Cross, J. B.; Bakken, V.; Adamo, C.; Jaramillo, J.; Gomperts, R.; Stratmann, R. E.; Yazyev, O.; Austin, A. J.; Cammi, R.; Pomelli, C.; Ochterski, J. W.; Martin, R. L.; Morokuma, K.; Zakrzewski, V. G.; Voth, G. A.; Salvador, P.; Dannenberg, J. J.; Dapprich, S.; Daniels, A. D.; Farkas, Ö.; Foresman, J. B.; Ortiz, J. V.; Cioslowski, J.; Fox, D. J. Gaussian, Inc., Wallingford CT, **2009**.
- [39] Cossi, M.; Rega, N.; Scalmani, G.; Barone, V. *J. Comput. Chem.* **2003**, *24*, 669-681.

TOC Entry



Isomeric benzodithiophenes in the core of a diethynyl bridge have a strong impact on the stability and electronic properties of oxidized diruthenium complexes.